STUDIES OF ATMOSPHERIC PROCESSES

Edward R. Fisher, et al

Wayne State University

Prepared for:

Air Force Cambridge Research Laboratories

15 December 1972

DOCUMENT CONTROL DATA - R & D

(Security classification of title, body of abstract and indexing annotation must be entered when the overall report is classified)

1. ORIGINATING ACTIVITY *(Corporate author)*	2a. REPORT SECURITY CLASSIFICATION
Wayne State University/College of Engineering Research Institute for Engineering Sciences Detroit, Michigan 48202	Unclassified
	2b. GROUP

3. REPORT TITLE

STUDIES OF ATMOSPHERIC PROCESSES

4. DESCRIPTIVE NOTES *(Type of report and inclusive dates)*

Scientific   Interim.

5. AUTHOR(S) *(First name, middle initial, last name)*

Edward R. Fisher   Pieter K. Rol
Ralph H. Kummler
Richard Marriott

6. REPORT DATE	7a. TOTAL NO. OF PAGES	7b. NO. OF REFS
15 December 1972	~~62~~ 63	35

8a. CONTRACT OR GRANT NO.	9a. ORIGINATOR'S REPORT NUMBER(S)
F19628-72-C-0007	Semi-Annual Technical Report No. 3
b. PROJECT NO. 8692 n/a n/a	
c. 62301D	9b. OTHER REPORT NO(S) *(Any other numbers that may be assigned this report)*
d. n/a	AFCRL-TR-73-0287

10. DISTRIBUTION STATEMENT

A - Approved for public release; distribution unlimited.

11. SUPPLEMENTARY NOTES	12. SPONSORING MILITARY ACTIVITY
"TECH, OTHER".	Air Force Cambridge Research Laboratories-OP L.G. Hanscom Field Bedford, Massachusetts 01730

13. ABSTRACT

This semi-annual report is divided into three separate sections; the first summarizes the conclusions reached in the experimental flow discharge facility concerning the deposition of energy into the internal modes of product molecules in simple combustion reactions, the second summarizes the progress in the theoretical close coupling vibrational relaxation cross sections appropriate to rarified flow regimes and the last section reviews the work to date in the molecular beam experiments aimed at determining the interaction potential for plume species.

DD FORM 1473 REPLACES DD FORM 1473, 1 JAN 64, WHICH IS
1 NOV 65   OBSOLETE FOR ARMY USE.

AD 769 996

KEY WORDS	LINK A		LINK B		LINK C	
	ROLE	WT	ROLE	WT	ROLE	WT
Energy Transfer Processes, Plume Chemistry, Chemiexcitation Processes						

STUDIES OF ATMOSPHERIC PROCESSES

by

Edward R. Fisher, Ralph H. Kummler, Richard Marriott

Pieter K. Rol

Research Institute for Engineering Sciences
College of Engineering
Wayne State University
Detroit, Michigan 48202

Contract No. F19628-72-C-0007
Project No. 8692

Semi-Annual Technical Report No. 3

15 December 1972

Contract Monitor: Alva T. Stair
Optical Physics Laboratory

Approved for public release; distribution unlimited.

Sponsored by

Advanced Research Projects Agency
ARPA Order No. 1856

Monitored by

AIR FORCE CAMBRIDGE RESEARCH LABORATORIES
AIR FORCE SYSTEMS COMMAND
UNITED STATES AIR FORCE
BEDFORD, MASSACHUSETTS 01730

Abstract

This semi-annual report is divided into three separate
sections the first summarizes the conclusions reached in
the experimental flow discharge facility concerning the
deposition of energy into the internal modes of product
molecules in simple combustion reactions, the second summarizes
the progress in the theoretical close coupling vibrational
relaxation cross sections appropriate to rarified flow
regimes and the last section reviews the work to date in
the molecular beam experiments aimed at determining the
interaction potential for plume species.

v

TABLE OF CONTENTS

l

Part I: INFRARED CHEMILUMINESCENCE FROM OXYGEN ATOM
ATTACK ON ETHYLENE

R.H. Kummler, Mazen Malki, and E.R. Fisher

Part I

Abstract

The 2.7μ emission from oxygen atom attack on ethylene has been studied in a discharge-flow tube system under conditions of low ethylene concentrations and excess oxygen atoms which favor the production of vibrationally excited $OH^{\dagger}$ at total pressures of about 1 Torr. The reactions responsible for this emission have been found to be

$$CHO + O \rightarrow CO + OH^{\dagger} \qquad (A)$$

followed by

$$OH^{\dagger} \rightarrow OH + h\nu \quad (7000A \text{ to } 2.7\mu)$$
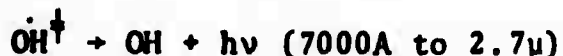
Another lesser but potentially important reaction at long contact times which may contribute to the $OH^{\dagger}$ is

$$CH_2O + O \rightarrow CHO + OH^{\dagger} \qquad (B)$$

An upper limit for k_B has been determined to be 3×10^{-14}.

The major loss mechanism for CHO in this system must be:

$$CHO + O_2 \rightarrow (products) \qquad (C)$$

and the ratio of the rate constants for reactions (A) and (C) was found to be $k_A/k_C \doteq 1.7 \pm 0.2$.

Introduction

The energy released in an exothermic chemical reaction can take several forms depending on the reaction path. The chemical energy of the reactants can be converted into translational energy of the products or it can be converted into internal energy of the products or some combination of both. The internal energy can be distributed among the electronic, vibrational, or rotational modes of the product molecule or molecules. If the product is elevated to a quantum state which has an optically allowed transition to a lower state, then the resulting light emitted permits the study of the reaction path leading to the internal energy. The observation of radiation associated with this non-equilibrium process thus provides information regarding the fundamental chemical kinetics of the reaction (e.g., Charters and Polanyi (1960); Polanyi, 1966; Polanyi, 1971; Hushafar, et al, 1971). It also provides the opportunity to assess the presence of one or both of the reactant partners in an unknown mixture of reactant gases. This capability is of considerable interest in the air pollution monitoring field and is applicable to both local and remote monitoring of exhaust gases (of rockets as well as automobiles) in the presence of an oxygen atom environment. In the spectral region of wavelengths from 1μ to roughly 15 or 20μ, the emitted light generally characterizes vibrational transitions which can result when the exothermic reaction produces a new bond in a heteronuclear molecule.

One common product of the combustion of hydrocarbons is

ethylene; oxygen atom attack on ethylene will produce a sequence of reactions between secondary species eventually producing several heteronuclear molecules with new bonds, especially OH and H_2O, which are strong radiators in the near infrared. Thus, we might expect to observe light emitted at the fundamental vibrational frequency of OH as well as the ν_3 mode of H_2O, both near 2.7μ. One of the early results of this work was the observation of emission at that wavelength. In order to apply the results of such observations to the sensing of the gaseous environment of interest, it is necessary to establish the molecular mechanism leading to the radiation because both the absolute concentrations as well as the ratio of reacting molecules in the field experiment may be considerably different than in the laboratory. With this in mind, the major task of this work was to establish the radiation contributing reactions and the major loss mechanisms for the observed infrared radiation In order to avoid competing reactions, it was decided that low concentrations of ethylene would be employed thereby avoiding reactions dependent upon more than one of the hydrocarbon frag- ments and in order to restrict the system to one radiator, vib- rationally excited OH (denoted hereafter by $OH^\dagger$ without regard to the details of the excitation). This process is necessary initially to simplify the reaction mechanism to a tractable point. The second major objective then becomes the quantifi- cation of the reaction system in terms of rate constants or quantum yields (ratio of photons emitted per molecule reacted) for the system.

The ethylene-oxygen atom system was chosen for this study because the ground state chemistry of the system is well known from the work of Niki, et al (1969), Stuhl and Niki (1971), Kanofsky, et al (1972), Atkinson and Cvetanovic (1972) and the intensive effort by the National Bureau of Standards culminating in the very accurate establishment of the rate constant for the primary step

$$O + C_2H_4 \rightarrow CHO + CH_3$$
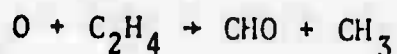
by Davis, et al (1972). Under these favorable conditions, the concentrations of the major species can be accurately modeled in the experimental system, and the rate constants for the radiating step can be obtained by essentially a perturbation analysis. This system was also chosen because of previous work by Krieger, Malki, and Kummler (1972) which identified $OH^{\ddagger}$ as a major radiator in the very near infrared (7000-9000A) under identical experimental conditions.

EXPERIMENTAL PROCEDURE

The oxygen atom attack on ethylene under 1 torr of total pressure was studied using a discharge flow system shown schematically in Figure (1).

The flow tube reactor is a 4 ft. long stainless-steel tube with a 1 inch I.D. teflon tube liner which aids in preventing wall recombination of some atomic species. It is provided with six ports for radial viewing through KCl windows (Harshaw Chemical Company). Two additional ports were used for measuring the absolute pressure and the drop in pressure across the reactor. Linear average velocities from 25 - 35 m/sec (with 33 m/sec being a typical velocity) were achieved when the pressure in the reactor was about 1 torr using a Heraeus Englehard (E-225, 147 cfm) mechanical pump. A Baratron (MKS type 77) capacitance manometer was employed to monitor the reactor pressure to better than 1μ accuracy.

The detectors used for this work were the PbS detector (Santa Barbara Research ATO type 8471-1) in conjunction with a phase sensitive lock-in amplifier (PAR HR8) for IR detection, and a photomultiplier detector (RCA C31025C) in conjunction with an electrometer (Keithley 602) for observation of visible emission.
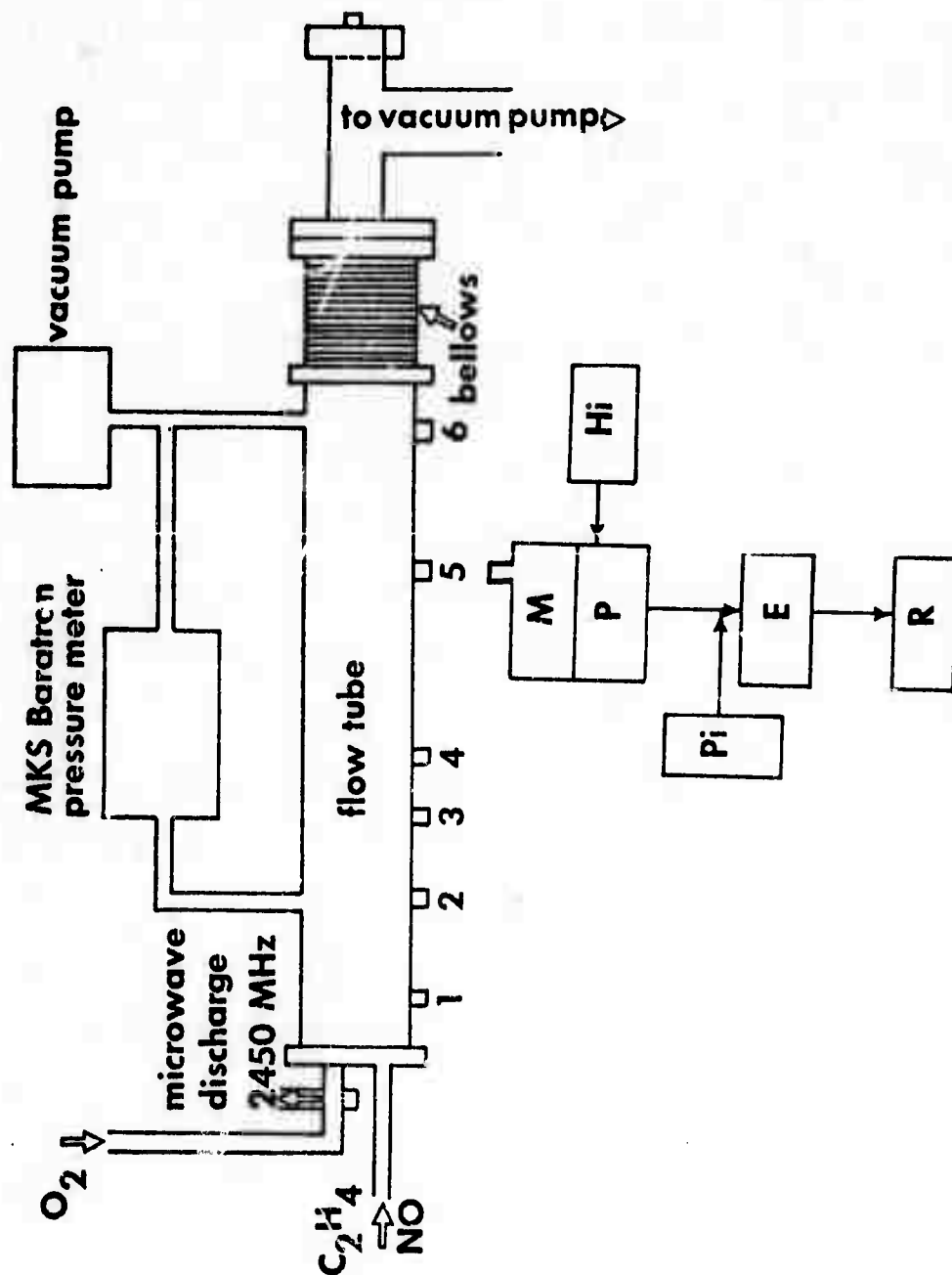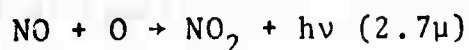
Figure 1. Schematic of Flow System. (M) is a monochromator used with the PbS detector (P), supplied by a high voltage power supply (Hi), E is the PAR HR8 phase sensitive lock in amplifier, and R the recording system.

In order to get absolute emission values, the system was calibrated using the reaction (Fontijn et al, 1964)

$$NO + O \rightarrow NO_2 + h\nu \ (2.7\mu)$$

for converting the arbitrary lock-in amplifier readings from μ volts to absolute photons/cc sec. The actinometric standard of Fontijn, et al was extended into the 2.7μ region using the data of Stair and Kennealy (1967).

The oxygen atoms were generated by passing oxygen (Cryogenic sales 99.6%) pure or diluted in argon (Cryogenic sales 99%) through an Evansen type cavity discharge powered by a 2450 MHz Raytheon PGM 10X2 diathermy unit.

The oxygen atoms were passed into the flow tube reactor through a closed end teflon tube with a radially multi-perforated exit stream. This permitted thorough mixing and a plug flow pattern at the point of mixing due to the turbulence caused by introducing the gas through a "showerhead" gas inlet. The plug on the end of the teflon piece served also to prevent the discharge region radiation from reaching the observation ports through scattering. The oxygen atom concentrations were measured by using the NO_2 titration technique (Kaufman 1961)).

It was found by using very small contrations of ethylene (on the order of < 1μ) complex hydrocarbon-hydrocarbon interactions could be eliminated significantly simplifying the kinetics and making the analysis of this system possible. A calibrated capillary provided the needed restriction on the C_2H_4 flow into

the reactor.

A steady state flow of the gas appropriate to the experiment (O_2 or O_2 + Ar) was obtained. Argon served to keep the pressure in the reactor constant allowing a reasonably constant linear velocity upon adding the ground state gas.

Thus, Argon, from a side gas inlet, **contributes most of the** pressure in the reactor (∿1 torr) while the ground state stream (NO, NO_2, C_2H_4) and the discharged stream (80μ O_2) are relatively small fractions of the total pressure.

The phase angle on the lock-in amplifier changed as one moved the PbS detector downstream and as the pressure changed in the flow tube. This had to be checked for all experimental data points. The reference to the PAR was taken from the pulse generator of the PGM 10X2. The pulse rate of the discharge was adjusted so that a single pulse of atoms traveled down the flow tube. This typically required repetition rates of 50 Hz to 100 Hz. The duty cycle for most measurements was 50%.

A run that involved the reaction NO + O → NO_2 + hν accompanied every set of data to put the lock-in amplifier readings on an absolute basis. A titration for oxygen atoms was also done as a part of the system calibration. The PbS detector with the PAR HR8 was used to monitor the intensity peak of the reaction NO_2 + O → NO + O_2 as a function of NO_2 concentration. **A sample** titration is given in Figure 2.

All observations of the O + C_2H_4 emission were made using the 2.7μ filter with transmission characteristics shown in Figure 3.
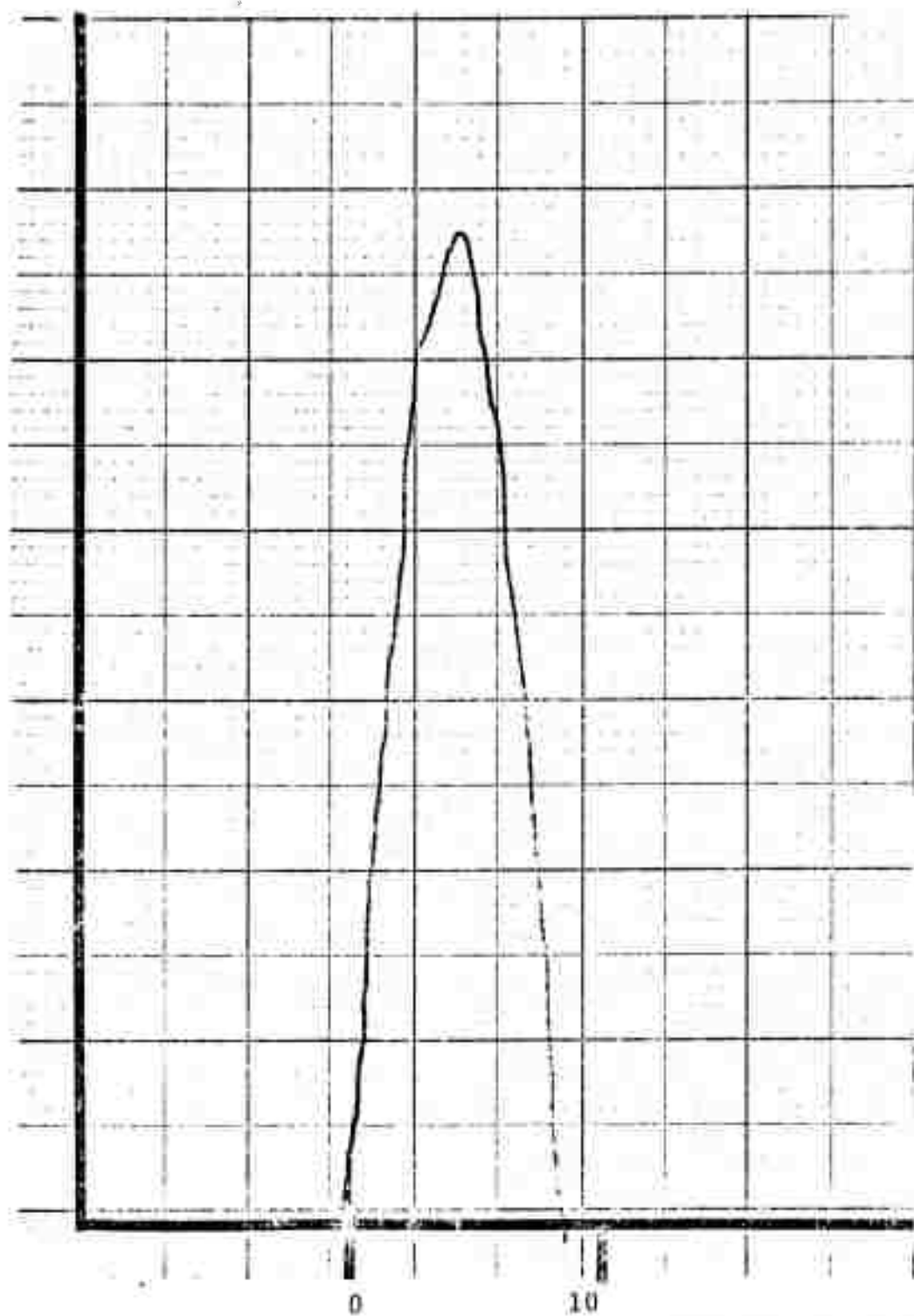
Figure 2. Titration of O using NO_2, observing the NO + O
glow with the PbS detector and the 2.7μ filter removed.
The contact time is 10.6 m sec, and the trace is taken on
the X-Y recorder.

-11-
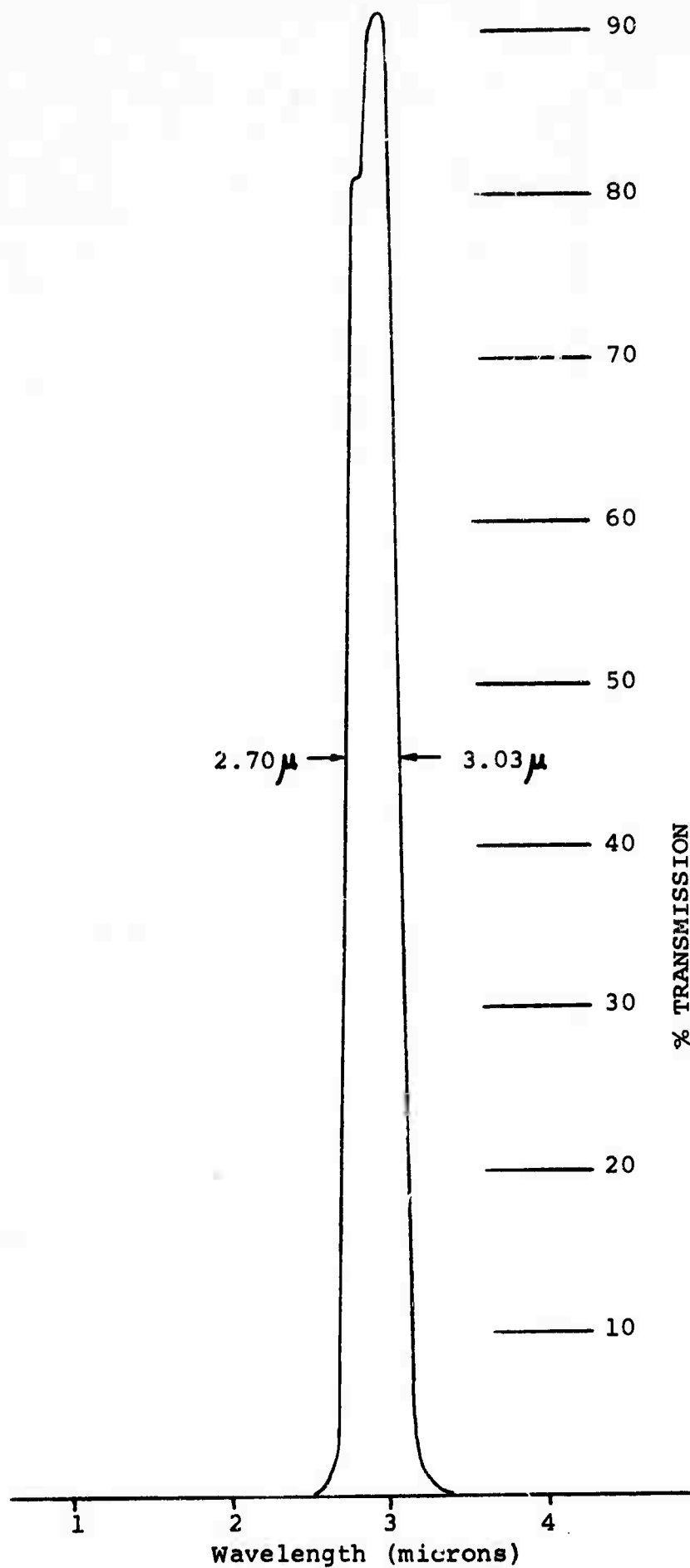
Figure 3: 2.7μ filter transmission curve

The linear velocity was measured using an oscilloscope (Tectronics type 556) to monitor the pulsed reference signal from the microwave generator. The scope also monitored the NO + O glow AC signal at a fixed port when NO was put in the system. Since the production of oxygen atoms was pulsed, and for these observations, the duty cycle was reduced to 10%, the NO + O glow signal was also pulsed. The delay between the production of the oxygen atoms and the observation of the signal, which could be viewed as the delay between the reference and the glow signal, was observed on the scope. This delay was related to the velocity in the reactor. Measurements at two different ports would give the delay time between pulses, and hence the velocity. A typical velocity vs. distance profile for the system is given in Figure 4.
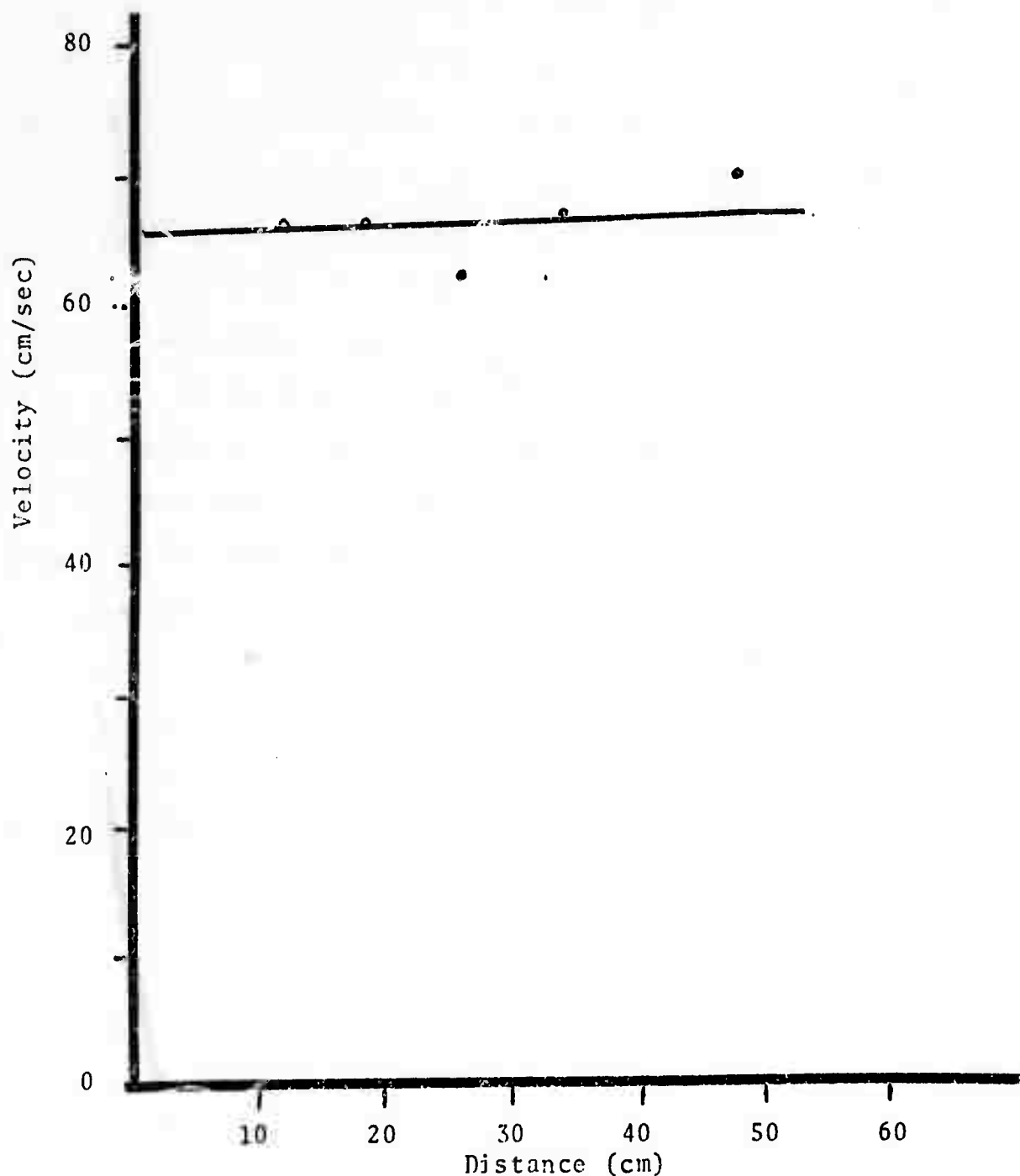
Figure 4. Velocity vs. distance downstream from the point of
reactant mixing. The total pressure is 0.96 Torr. The error
in the measurement is greatest between the first two windows.
Thus, the velocity appears to be essentially constant down
the flow tube, which implies a constant density system.
The velocity measurement made is the centerline velocity from
bolus washout theory. The average velocity is half of this
value.   -14-

THE MECHANISM

General

The reaction of oxygen atoms with ethylene has been
phenomenologically found to produce infrared radiation, at
least partly in the 2.7µ region. The major effort of this
work is devoted to the quantitative explanation of that radi-
ation in forms of the detailed molecular mechanism. The gen-
eral ground state system of intermediates resulting from the
combination of O and C_2H_4 is well established primarily from
the discharge-flow-tube-time-of-flight mass spectrometric study
of Niki et al (1969) and the direct observation of the products
CH_3 and CHO in the high intensity crossed beam experiment of
Kanofsky et al (1972). These two studies along with the simi-
lar flow tube mass spectrometric work of Herron and Penzhorn
(1969) have established that the primary elementary step (90%)
in the reaction mechanism is

$$O + C_2H_4 \rightarrow CH_3 + CHO \qquad (1)^*$$

Other minor species were observed by Kanofsky, et al (1972),
but notably, the production of CH_2 and H_2CO were not observed
to occur in the primary step. The eventual stable products
formed by secondary reactions include H_2CO, CO, H_2, O_2, and H.
Consideration of the temporal behavior of these products as well

---

* Numbering refers to Table II.

as isotopic experiments led Niki, et al (1969) to postulate
that the following reactions occur:

$$CH_3 + O \rightarrow HCHO + H \tag{2}$$

$$CHO + O \rightarrow CO + OH \tag{4}$$

$$HCHO + O \rightarrow CHO + OH \tag{17}$$

$$CHO + O \rightarrow CO_2 + H \tag{5}$$

$$OH + O \rightarrow O_2 + H \tag{6}$$

$$CHO + H \rightarrow H_2 + CO \tag{7}$$

Water was not observed to be a product of this system by Niki,
but his system employed very small concentrations of C_2H_4 with
O in excess, so that the OH concentration and hence the rate
of the reaction:

$$OH + OH \rightarrow H_2O + O \tag{11}$$
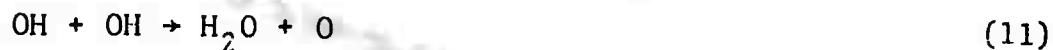
were both small. In a more general case, H_2O might be a sig-
nificant product.

Both OH and H_2O are produced by exothermic reactions in
the above sequence under conditions where each is the new bond
formed by a neutral rearrangement reaction. Under conditions
such as this, it is well established that a significant frac-
tion of the exothermicity of the reaction can appear as vib-
rational energy in the new bond (Smith (1972); Pacey and Polanyi
(1971); McGrath and Norrish (1957); Parker and Pimentel (1969);
Jonathan, et al (1971); Stair and Kennealy (1967); Hushfar, et
al (1971) and many others).

TABLE II

	Reaction	Rate Constant, 300°K	Reference	$\Delta H_r \frac{k\ cal}{gmole}$
1	$C_2H_4 + O \rightarrow CH_3 + CHO$	8.42^{-13}	Davis, et al (1972)	-42.45
2	$CH_3 + O \rightarrow HCHO + H$	3.0^{-11}	Niki, et al (1969)	-66.54
3	$HCHO + O \rightarrow CHO + OH^{\ddagger}$		Calculated	
4	$CHO + O \rightarrow CO + OH$	1.0^{-12}	Niki, est.	-73.09
5	$CHO + O \rightarrow CO_2 + H$	3.0^{-13}	Niki, est.	-98.05
6	$OH + O \rightarrow O_2 + H$	5.0^{-11}	Kaufman (1964)	-16.79
7	$CHO + H \rightarrow CO + H_2$	4.0^{-12}	Niki, et al (1969)	-75.62
8	$OH^{\ddagger}_{(v=1)} \rightarrow OH + h\nu$	3.3	Potter, et al (1971)	
9	$CHO + O_2 \rightarrow CO + HO_2$	2×10^{-13}		-18.88
10	$OH^{\ddagger} + O \rightarrow O_2 + H$	5.0^{-11}	Kaufman (1964)	
11	$OH + OH \rightarrow H_2O + O$	2.5^{-12}	Dixon-Lewis et al (1966)	-16 95
12	$OH + OH \rightarrow H_2O^{\ddagger} + O$	2.5^{-13}	Estimate	
13	$CH_3 + O_2 + M \rightarrow CH_3O_2 + M$	8.0^{-32}	Heicklen	
14	$H + O_2 + M \rightarrow HO_2 + M$	3.0^{-32}	Kaufman (1964)	-47.4
15	$H_2O^{\ddagger} + M \rightarrow H_2O + M$	1.0^{-12}	Estimate	
16	$H_2O^{\ddagger} \rightarrow H_2O + h\nu$	30	Penner (1959)	
17	$HCHO + O \rightarrow CHO + OH$	1.6^{-13}	Niki, et al (1969)	-24.77
18	$CHO + O \rightarrow CO + OH^{\ddagger}$		Calculated	

20	$OH + HCHO \rightarrow H_2O^{\ddagger} + CHO$	1.4^{-12}	Estimate	
21	$OH + H_2 \rightarrow H_2O + H$	6.6^{-15}	Greiner (1969)	-119.234
22	$OH + HO_2 \rightarrow H_2O + O_2$	1.0^{-11}	Kaufman (1964)	-71.87
23	$HO_2 + O \rightarrow OH + O_2$	1.0^{-11}	Lloyd (1970)	-54.2
24	$H + HO_2 \rightarrow OH^{\ddagger} + OH$	1.0^{-12}	Crutzen (1971)	-38.4
25	$OH + HO_2 \rightarrow H_2O^{\ddagger} + O_2$	1.0^{-12}	Estimate	
26	$C_2H_4 + O \rightarrow CH_3 + CHO^{\ddagger}$	5.2×10^{-14}	Estimate	
27	$CHO^{\ddagger} + O \rightarrow CO + OH^{\ddagger}$	1.0^{-11}	Estimate	
28	$H + HO_2 \rightarrow OH + OH$	1.0^{-11}	Estimate	
29	$O + HO_2 \rightarrow OH^{\ddagger} + O_2$	1.0^{-12}	Estimate	
30	$CO + OH \rightarrow CO_2 + H$	1.5^{-13}	Wilson (1972)	
31	$OH^{\ddagger} + O_2 \rightarrow O_2 (b^1\Sigma_g) \, OH$	3×10^{-14}	Potter, et al	
32	$OH^{\ddagger} + H \rightarrow H_2 + O$	1×1.0^{-12}	Estimate	
33	$O_2 (b^1\Sigma) + O_2 \rightarrow O_2 + O_2$	3×10^{-16}	Estimate	
34	$O_2 (b^1\Sigma) + O \rightarrow O_2 + O$	2×10^{-13}	Estimate	
35	$O_2 (b^1\Sigma) + H \rightarrow O_2 + H$	2×10^{-13}	Estimate	
36	$H + HCHO \rightarrow H_2 + CHO$	1×10^{-13}	Westenburg and Dehaas (1972)	
37	$CHO^{\ddagger} + O_2 \rightarrow CO + HO_2$	1×10^{-11}	Estimate	
38	$O \rightarrow 1/2 \; O_2$	137	Estimate, wall deactivation	
39	$H \rightarrow 1/2 \; H_2$	137	Estimate	
40	$OH^{\ddagger} \rightarrow OH$	137	Estimate	
41	$H_2O^{\ddagger} \rightarrow H_2O$	137	Estimate	
42	$CHO^{\ddagger} \rightarrow CHO$	137	Estimate	
43	$O_2 (b^1\Sigma_g) \rightarrow O_2 (X^3\Sigma)$	137	Estimate	
44	Dummy			
45	$OH^{\ddagger} + M \rightarrow OH + M$	1.5×10^{-14}	Estimate	
46	$OH^{\ddagger} + H_2 \rightarrow H_2O + H$	1×10^{-14}	Estimate	
47	$C_2H_4 + OH \rightarrow CH_3 + HCHO$	1.8×10^{-12}	Morris & Niki (1971)	
48	$OH^{\ddagger} + C_2H_4 \rightarrow$			

Thus, in the general case, both the OH fundamental and the H_2O ν_3 band could be expected to contribute to emission near 2.7μ. In order to simplify the initial kinetic system, it was decided to work at small C_2H_4 concentration in order to minimize the $H_2O^{\ddagger}$ production. In addition, the O_2 concentration was minimized in order to avoid the reactions

$$H + O_2 + M \rightarrow HO_2 + M \tag{14}$$

$$O + HO_2 \rightarrow OH^{\ddagger} + O_2 \tag{29}$$

$$H + HO_2 \rightarrow OH^{\ddagger} + OH \tag{24}$$

$$OH + HO_2 \rightarrow H_2O^{\ddagger} + O_2 \tag{25}$$

The minimization of the C_2H_4 also prevented significant contributions from

$$OH + C_2H_4 \rightarrow products \tag{47}$$

$$OH + H_2 \rightarrow H_2O^{\ddagger} + H, $$
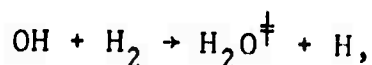
as well as minimizing the contribution of

$$OH^{\ddagger} + C_2H_4 \rightarrow products \tag{48}$$

$$OH^{\ddagger} + HC - fragment \rightarrow products$$
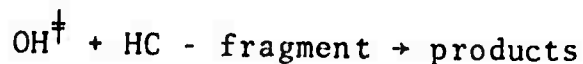
to the $OH^{\ddagger}$ loss. Under such circumstances, the major $OH^{\ddagger}$ loss process will be via

$$OH^{\ddagger} + O \rightarrow O_2 + H, \tag{10}$$

which is extremely fast, even for the ground state OH molecule. In fact, reaction with O as a homogeneous loss process is so

rapid that $OH^{\ddagger}$ deactivation on the wall, which would be diffusion controlled even if every wall collision were effective in de-activation, can be neglected. However, it was found that, in the general case small additional loss mechanisms provided by

$$OH^{\ddagger} + O_2 \rightarrow O_2(^1\Sigma_g) + OH \tag{31}$$

and

$$OH^{\ddagger} + M \rightarrow OH + M$$
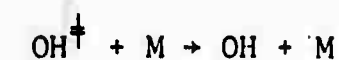
were needed to fit the observed data at long contact times.

The problem of analyzing the relative role of each reaction in the complete mechanism of Table II was approached both numerically and analytically. In the former method, all the reactions were included and the resulting differential equations were integrated using the Keneshea (1967) code which incorporates the Runge Kutta Merson integration procedure with a steady state linearization-iteration algorithm which is implemented when the equations become stiff. This is a standard procedure previously employed for such problems (Kummler and Bortner, 1968; Gutowski, 1971; Roginsky, 1972). The numerical integration was employed for two purposes. First, Hypotheses regarding the relative importance of the various reactions and species could be readily tested under prototype conditions and the experimental conditions could be adjusted to optimize the desired measurement. Second, consistency between the final predicted and calculated intensities could be obtained.

It was found that $H_2O^{\ddagger}$ emission strongly increased when the C_2H_4 concentration in the system exceeded a few microns, and became insignificant at concentrations of C_2H_4 less than 1μ as shown in Figures 5 and 6 from the numerical model. Using the capillary tubing provided the needed restriction to the C_2H_4 flow into the reactor and allowed the introduction of C_2H_4 partial pressures as low as 0.1μ at a 1 torr total pressure in the flow system.
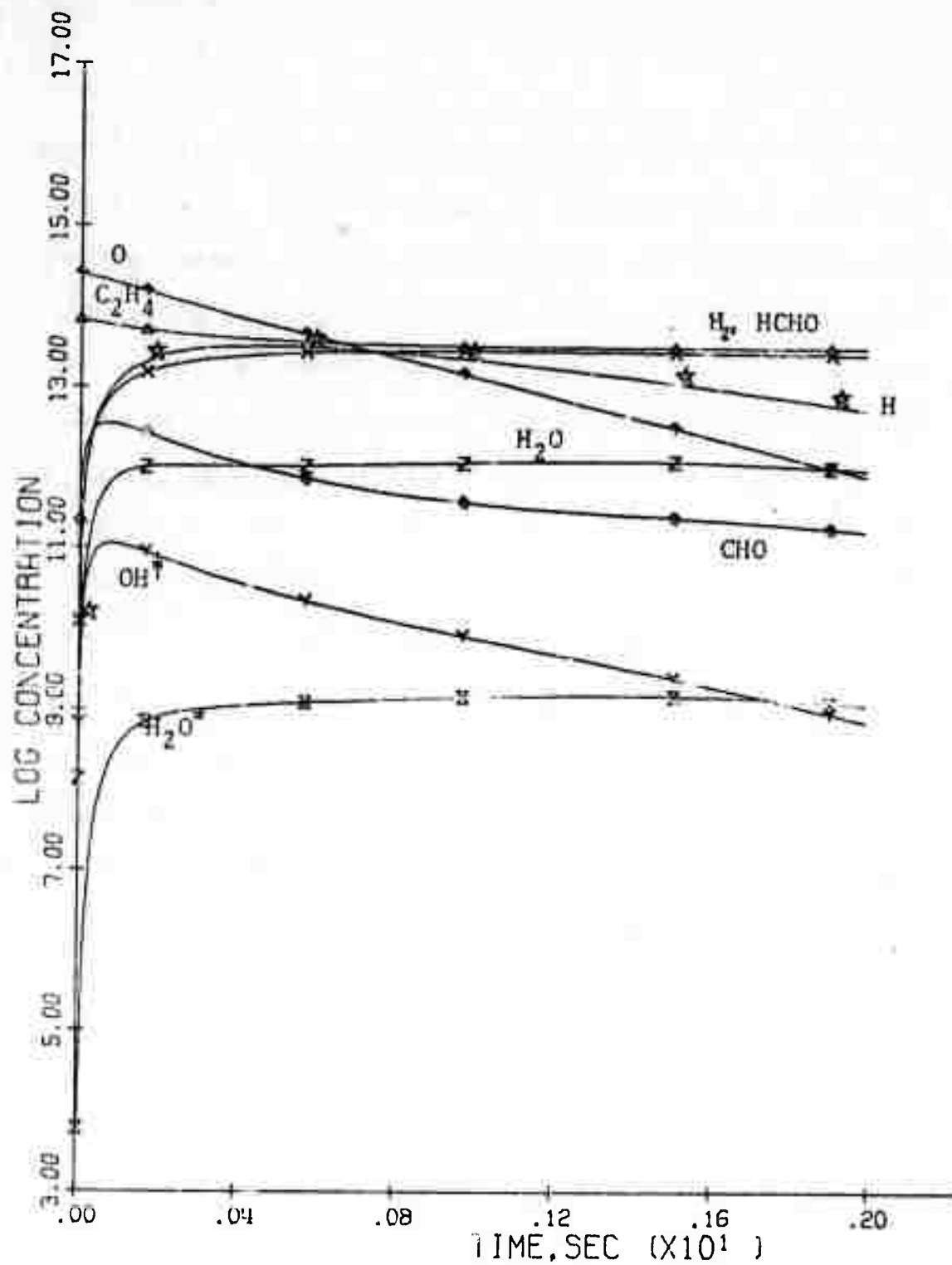
Figure 5. The log of the concentrations of the species of major interest at high C_2H_4 concentration as a function of reaction time.
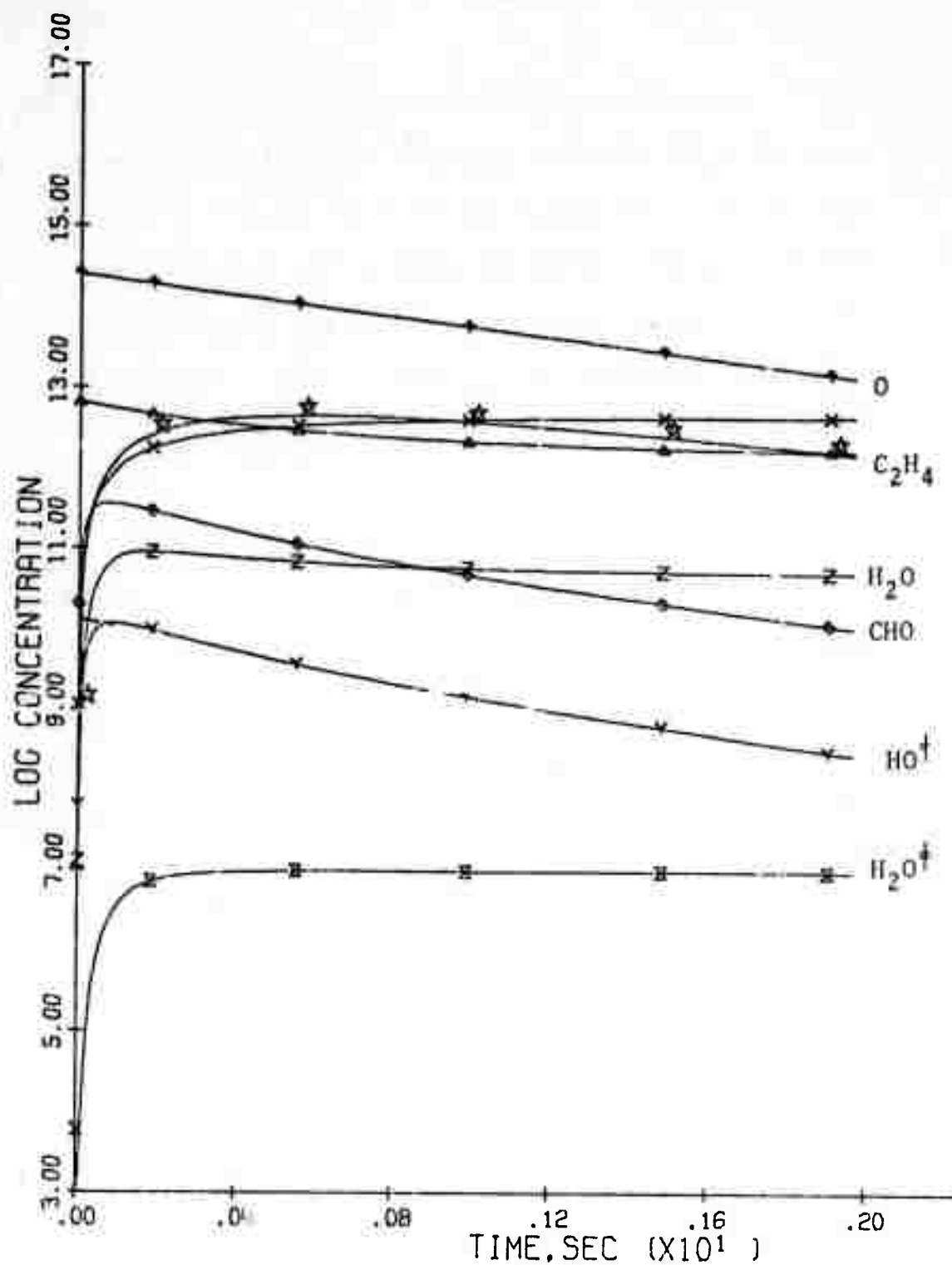
Figure 6. The major species concentrations at low C_2H_4 concentration as a function of reaction time.

Assuming experimental conditions preventing the formation of $H_2O^{\ddagger}$ and favoring $OH^{\ddagger}$ as in Figure 6, we can examine the reaction mechanism as shown in Figure 7. Oxygen atoms plus ethylene yield the methyl and formyl radicals, CH_3 and CHO. Then, $OH^{\ddagger}$ production occurs via two routes. The first is the immediate reaction of the formyl radical produced in the primary step:

$$O + CHO \rightarrow CO + OH^{\ddagger}, \tag{18}$$

which is extremely rapid (Browne, et al, 1971). CHO is also lost by the rapid process:

$$CHO + O_2 \rightarrow products \tag{19}$$

which will dominate at high O_2 concentrations. With the steady state postulate on CHO, for purposes of this data analysis, the rapidity of this reaction permits the reaction to be conceptualized in the following way. The reaction mechanism is equivalent to the introduction of CHO rather than C_2H_4 since the steady state immediately converts the CHO to $OH^{\ddagger}$ with no time lag. The rapid steady state also occurs for the methyl radical which is lost via

$$O + CH_3 \rightarrow H_2CO + H \tag{2}$$

The result of the oxygen atom plus methyl radical does not, however, result in direct production of $OH^{\ddagger}$. As shown

-24-

in Figure 7, the $OH^{\ddagger}$ results from the relatively slow subsequent process

$$O + H_2CO \rightarrow CHO + OH^{\ddagger}, \tag{3}$$

and the CHO also reacts with O as above to produce an additional $OH^{\ddagger}$. Because reaction 3 is slow, all $OH^{\ddagger}$ produced via the CH_3 primary product will exhibit a time lag, whereas the $OH^{\ddagger}$ produced from the formyl radical which is a primary product will exhibit no apparent time lag. This suggests a method of obtaining both quantum yields from analysis of the radiation as a function of flow tube position. While the numerical solution illustrated in either Figure 5 or 6 indicates a rapid rise of $OH^{\ddagger}$ and CHO from zero at zero time. extrapolation of the $OH^{\ddagger}$ curve indicated by the dotted line in Figure 6 will yield an intercept which represents the $OH^{\ddagger}$ production due to the hypothetical introduction of CHO at zero time. This intercept, as shown below, permits the obtention of the rate constant, k_{18}, for the reaction

$$O + CHO \rightarrow CO + OH^{\ddagger}. \tag{18}$$

Analysis of the data for long contact times permits estimation of the rate reaction 3,

$$O + CH_2O \rightarrow OH^{\ddagger} + CHO. \tag{3}$$

This division of time zones is supported by the work of Krieger,

OXYGEN ATOM ATTACK ON ETHYLENE

Figure 7. Schematic of the Reaction Mechanism Proposed
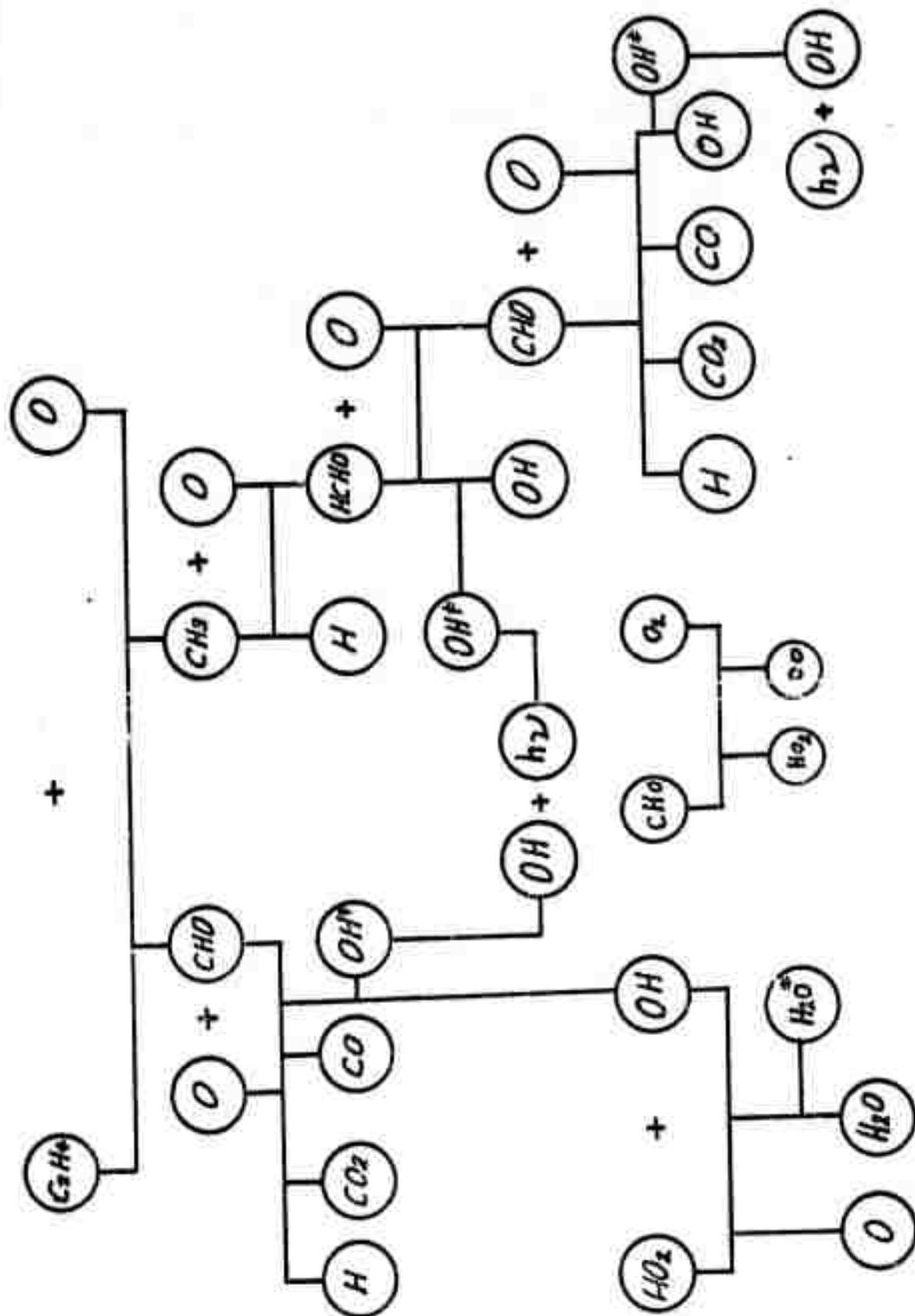
Malki and Kummler (1972), who found that the OH Meinel bands
($v' \sim 7$ to 9) were produced early in the flow system as shown
in Figure 8.
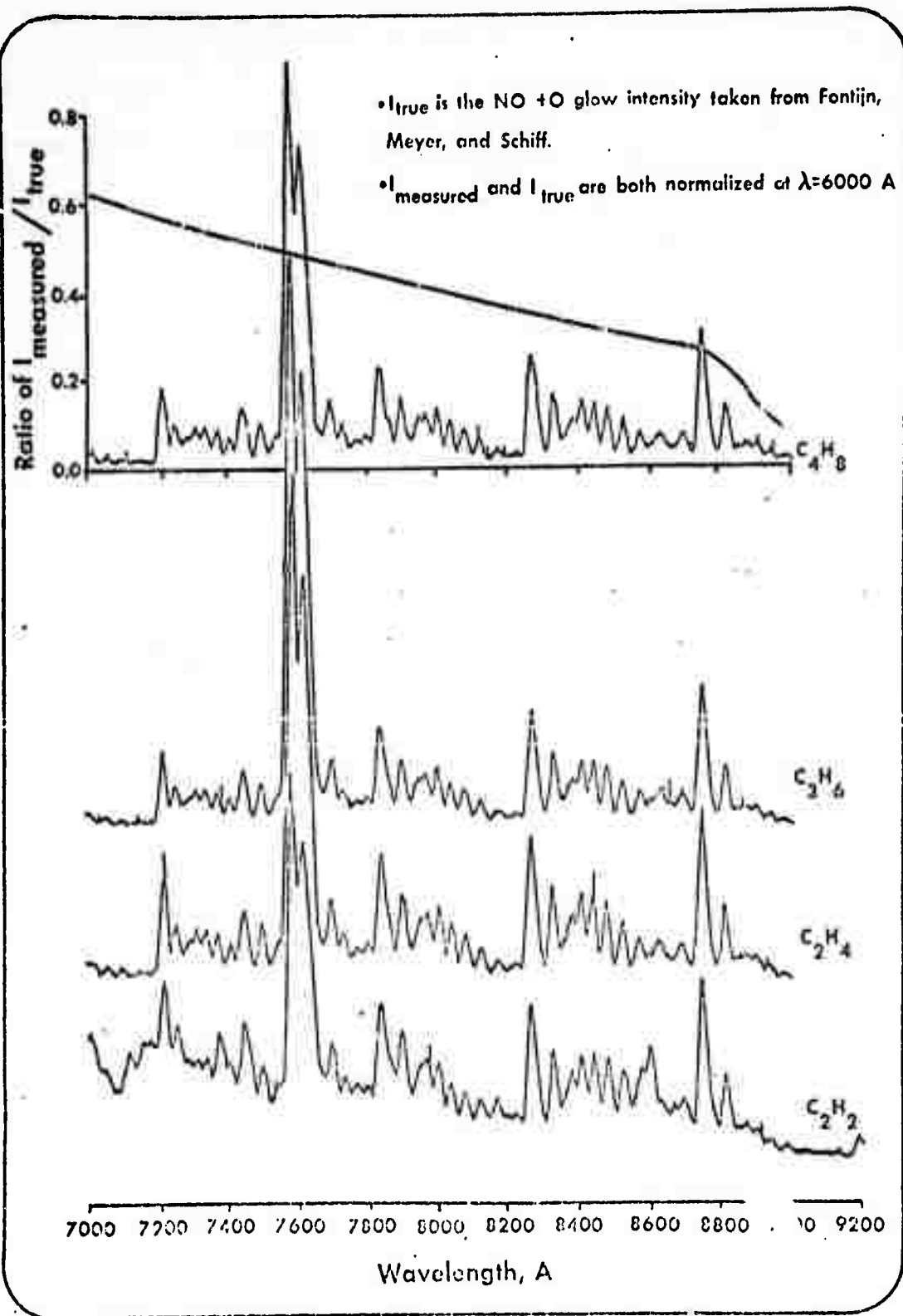
Figure 8.   Meinel bands of OH for the attack of O on C_2H_4 at short contact time ($\sim$ 1-3 m sec) taken from Krieger, Malki and Kummler (1972).   The total pressure is 1.28 Torr and the hydrocarbon partial pressure is 20 millitorr.

The Analytical Solution

First, the steady state assumption will be invoked for $OH^{\ddagger}$ because the time constant for the loss mechanism for $OH^{\ddagger}$,

$$OH^{\ddagger} + O \xrightarrow{k_{10}} O_2 + H, \tag{10}$$

is small compared to the reactor contact time. k_{10} may be estimated in two ways. First, we will assume that the lower bound is the rate constant for

$$OH + O \rightarrow O_2 + H \tag{6}$$

as determined by Kaufman (1964) and by Clyne (1963): $k_{10} = 5 \times 10^{-11}$ cc/sec. Thus, at a typical oxygen atom number density of 2×10^{14} 1/cc, the effective first order rate constant for the loss of $OH^{\ddagger}$ is 10^4, or the time constant for $OH^{\ddagger}$ loss is 0.1 msec. compared to the contact time at the first window of 2.42 msec. Other potential loss mechanisms, such as

$$OH^{\ddagger} + OH \rightarrow H_2O + O$$

and

$$OH^{\ddagger} + H_2 \rightarrow H_2O + H$$

$$OH^{\ddagger} \rightarrow OH + h\nu \tag{8}$$
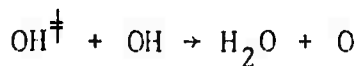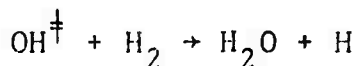
are at least 10 times slower under most experimental conditions employed in the present study.

The upper limit for k_{10} would be the gas kinetic rate constant,

$$k = \pi \sigma^2 \sqrt{\frac{8RT}{\pi \mu}}$$

where for this system

$$\sigma_{OH} = 3A, \quad M_{OH} = 17$$

$$\sigma_0 = 1.3A, \quad M_0 = 72, \quad R = 8.3 \times 10^8, \quad T = 300°K$$

$$\therefore \sigma_{OH-O} = 2.2A, \quad \mu = .236^{-1}$$

$$k_{10} = 1.7 \times 10^{-10} \text{ cc/sec}$$

The lower limit is taken to be the value of k_{10}. Thus, from Table II, in the steady state,

$$OH^{\ddagger} = \frac{k_3[H_2CO][O] + k_{18}[CHO][O] + k_{24}[H][HO_2] + k_{29}[O][HO_2]}{k_{10}[O]} \tag{1}$$

Reaction 24 is found not to be important in the mechanism. An experiment that proved the ineffectiveness of reaction 29 was carried out. Molecular ground state oxygen that would enhance the production of HO_2 via reactions 9 and 14 did not increase the $OH^{\ddagger}$ (2.7µ) emission as reaction 29 suggested. One could therefore conclude the quantum yield of reaction 23 was not appreciably important. Thus, equation (1) reduces to:

$$OH^{\ddagger} = \frac{k_3 \cdot CH_2O + k_{18} \cdot CHO}{k_{10}} . \tag{1a}$$

-30-

Under these assumptions and the postulate: $(k_9) \cdot O_2 > (k_4 + k_5) \cdot O$
which is the only condition consistent with the data, we can
compute the $OH^{\ddagger}$ concentration.

Neither k_4, k_5, nor k_9 are well known. The above
reduces the steady state equation for CHO to

$$CHO = \left(\frac{k_1\ C_2H_4 + k_{17}\ CH_2O}{k_9\ O_2} \right) \cdot O \tag{8}$$

The molecular oxygen concentration is constant down the
tube as described by the computer model. This allows us to
write, upon substituting the time dependency in equation (8):

$$CHO = \frac{k_1 C_2H_4|_0 \{ e^{-k_1' \int O dt} \cdot (-2k_{17}+k_1) + k_{17} e^{-k_{17} \int O dt} \} \cdot O}{k'_1\ k_9\ O_2} \tag{9}$$

where

$$k'_1 = k_1 - k_{17}$$

Guided by the numerical integration that describes this
approach, the formaldehyde concentration is considered to be con-
stant down the tube. It is reasonable to predict a small,
slowly increasing, contribution to the emission from this species
according to

$$I\Big|_{\substack{\text{due to} \\ CH_2O}} = \frac{k_1 C_2H_4|_0}{k'_1} \left(e^{-\int k_{17} \cdot O \cdot dt} - e^{-\int k_1 \cdot O \cdot dt} \right) \cdot \frac{A_m\ k_3}{k_{10}} \tag{10}$$

The exponential function of the second term is larger than that of
of the first. This should give a small upward trend in the
intensity.

-31-

This small rise is not significant when compared to the contribution from CHO

$$I\Big|_{\substack{\text{due to} \\ \text{CHO}}} = \frac{A_n \cdot k_{18} \cdot k_1 \cdot C_2H_4\Big|_0}{k_{10} \cdot k'_1 k_9 O_2} \Big[e^{-k_1 \int O dt} (k_1 - 2k_{17})$$

$$e^{-k_{17}\int O dt} \cdot k_{17}\Big] \cdot O\Big|_o e^{-k_w t} \tag{11}$$

where k_w = wall recombination (of oxygen atoms) rate constant.

Both the increase of $\int O dt$ and the decrease of the oxygen atom concentration due to wall recombination reduces the intensity as a function of time.

This is best represented by the expression

$$\log_{10} I = \log_{10} A - k_w t \tag{11a}$$

where

$$A = \frac{A_n k_{18} k_1 \cdot C_2H_4\Big|_0}{k_{10} k'_1 k_9 O_2} \cdot O\Big|_0 \Big[e^{-k_1 \int O dt} (k_1 - 2k_{17}) +$$

$$e^{-k_{17}\int O dt} \cdot k_{17}\Big] \tag{12}$$

The time dependency of A is small and will give an approximate log linear equation over the range of interest. This explains the semi log straight line relationship which appears to fit experimental data.

The approximation of constant $\int O\,dt$ does not effect the accuracy of the calculated k_{18}. It is illustrated earlier that an intercept when $t = 0$ is a valid concept and is equivalent to a hypothetical introduction of CHO at time zero. Equation 12 reduces to

$$\log_{10} I = \log_{10} \frac{A_n k_{18} k_1 C_2H_4|_0}{k_{10} \cdot k_9 O_2} \cdot O|_0$$

and

$$A_n \cdot \frac{k_{18}}{k_9} = \frac{I \; k_{10} \; O_2}{O \; k_1 \; C_2H_4|_0} \tag{13}$$

At the end of the tube when CHO production decreased to a great extent due to the wall recombination of the oxygen atoms, the only significant radiation would be due to formaldehyde. This argument could be used to place an upper limit on K_3. The intensity at the last window is taken to be the limit corresponding to the highest possible k_3 (from equation 11):

$$k_3 = \frac{I|_{\text{limit}} \cdot k'_1 \cdot k_{10}}{k_1 C_2H_4|_0 \; (e^{-\int k_{17} O\,dt} - e^{-\int k_1 O\,dt}) \; A_m} \tag{14}$$

where

$$I|_{\text{limit}} = \text{the maximum intensity due to } CH_2O$$

A plot of intensity vs. C_2H_4 at constant contact time is obviously expected to give a straight line relationship. The curvature in the experimental data presented in the results

section is attributed to the small dependence of the oxygen atoms on ethylene. This dependence becomes least important at low ethylene concentration. Thus an initial slope of the data is a good approximation of the slope described by equation (11):

$$\text{Slope} = \frac{A_n \cdot k_{18} \cdot k_1}{k_{10} \cdot k_1 \cdot k_9 O_2} \cdot O|_0 \left(e^{-k_1 \int O dt} (k_1 - 2k_{17}) + e^{-k_{17} \int O dt} \cdot k_{17}\right) \cdot e^{-k_w t} \tag{15}$$

The term $\int O dt$ is calculated numerically. k_w is the wall recombination rate constant of oxygen atoms. k_w is calculated by observing the NO + O glow signal decay down the tube.

Results and Discussion

It has been proposed that the reaction

$$CHO + O \rightarrow CO + OH^{\ddagger} \; (2.7\mu) \tag{18}$$

is primarily responsible for the emission in the flow tube system. It has also been postulated that the reaction

$$CH_2O + O \rightarrow CHO + OH^{\ddagger} \; (2.7) \tag{3}$$
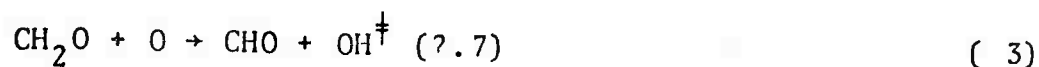
would predominate at longer contact times due to the decrease of the oxygen atom concentration (see equation 10 and 11 in the previous section).

Under this mechanism, in which CHO is primarily lost by reaction with O_2, it is predicted, as shown in Figures 9 and 10 that the observed intensity should be nearly proportional to the C_2H_4 concentration, until C_2H_4 reacts significantly with and therefore depletes the O atom concentration.

In Figures 9 and 10, the solid line represents the theoretical prediction of the computer model and the points represent the experimentally obtained OH* concentration using the actinometric standard of the NO + O glow as determined by Fontijn, et al. The rate constants for the computer fit are obtained using the analytic solution for Postulate 3, based on the data of June 15 (Figure 9) as previously described. The computer code is then used to predict the data of June 12 which has a higher oxygen atom concentration as well as a higher O_2 concentration (Figure 10).

Figure 9. A comparison of the theoretical prediction vs. the experimental data at 2.7μ. The initial O concentration is 7.8μ and the initial O_2 is 80μ. The solid line is the theoretical prediction (the last point identifies the contact time) and the unconnected points are the experimental data of June 15, 1972.
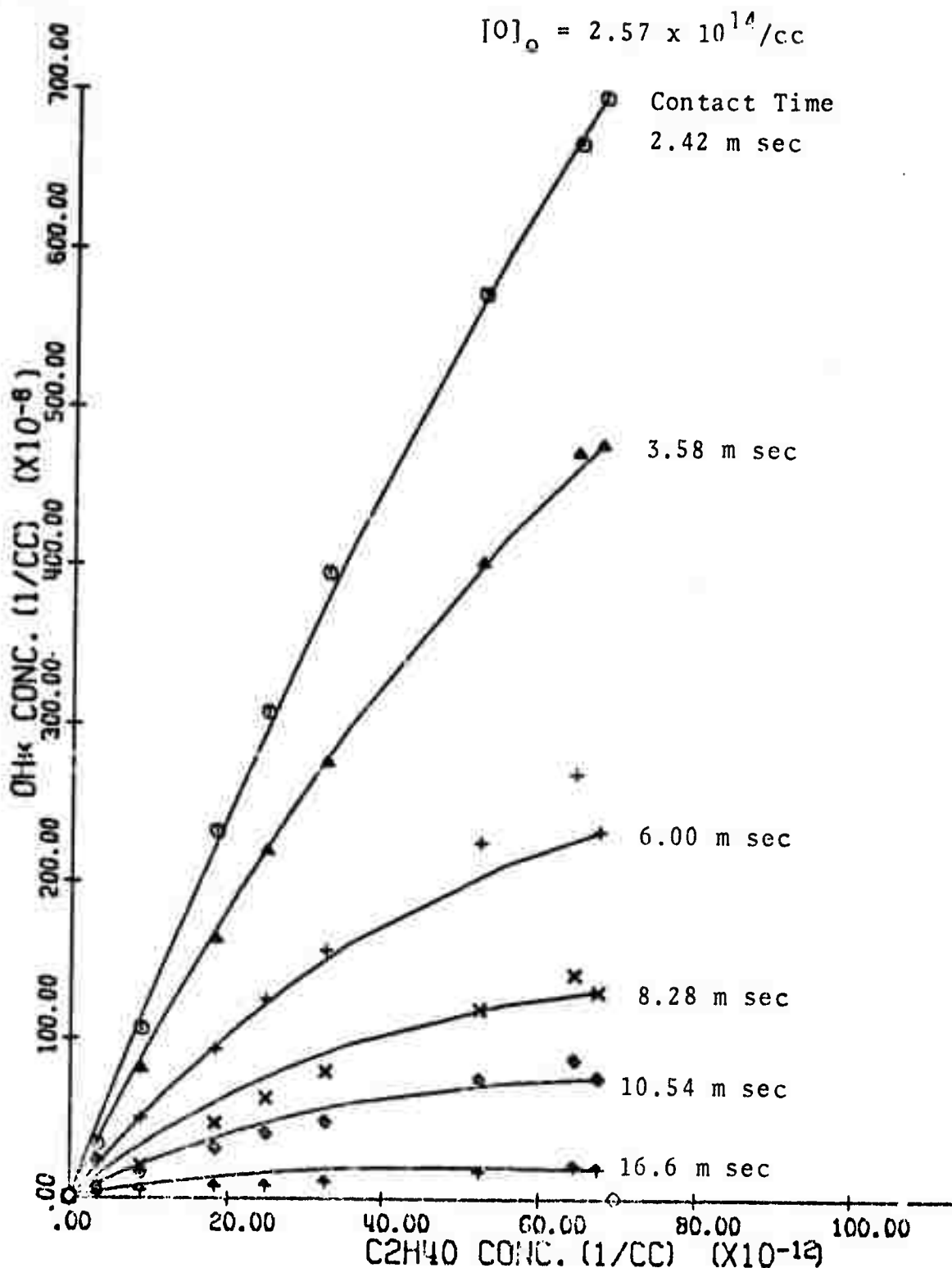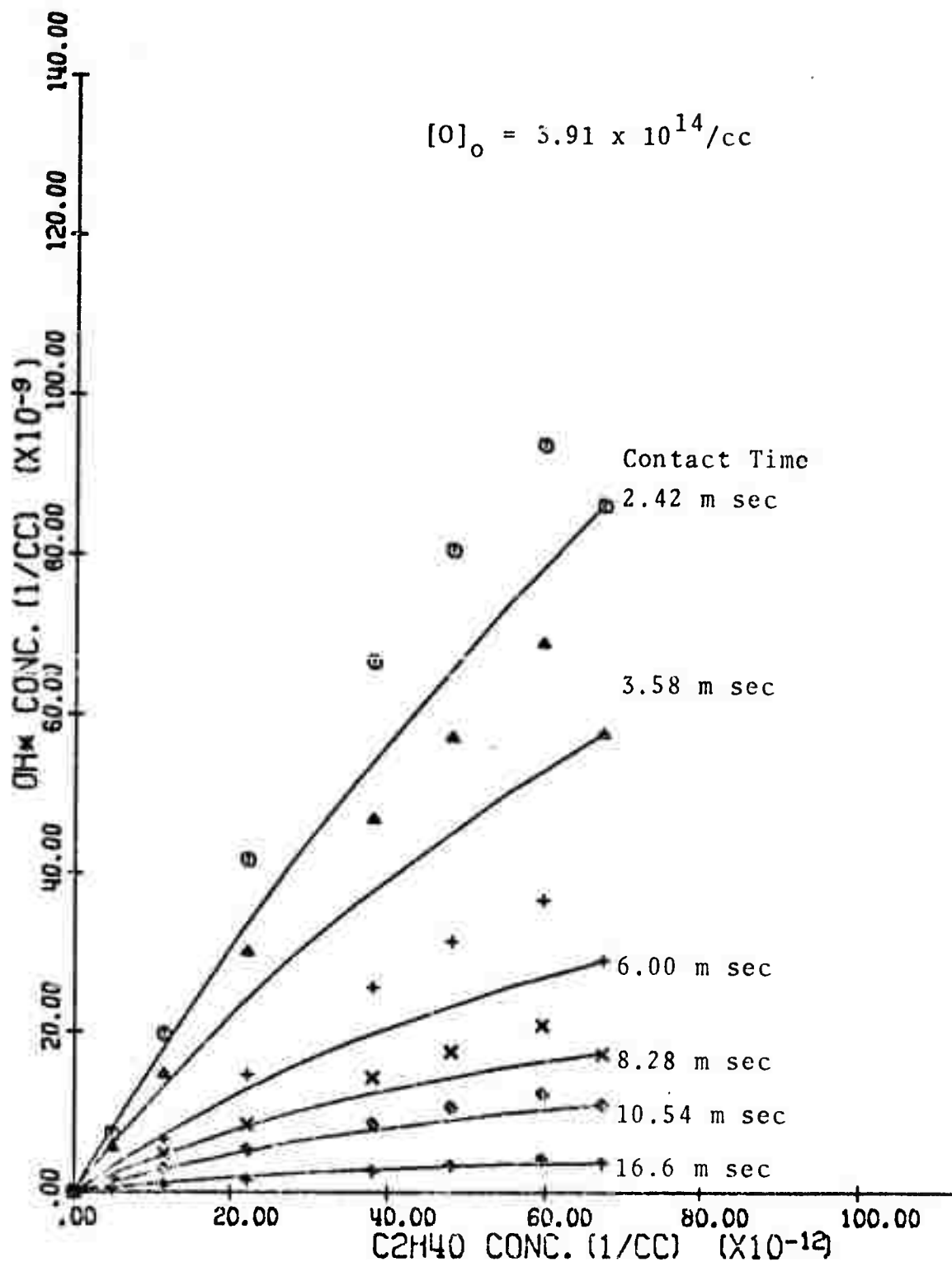
Figure 10. A comparison of the theoretical prediction vs. the experimental data at 2.7μ. The initial O concentration is 11μ and the initial O_2 is 88μ. The data were taken on June 12, 1972.

The experimental data shows some deviation at higher ethylene concentrations and short times where significant deviations from the proposed mechanism are expected to appear because of $H_2O^{\ddagger}$ emission, but the data generally verify the expected proportionality between observed intensity and initial C_2H_4 concentration over an order of magnitude in concentration and time.

A plot of $\log_{10}$ (intensity) vs. time should enable two pieces of information to be obtained: a value for $\frac{k_{18}}{k_9}$ and an upper limit on k_3. Figure 11 represents the typical plot of the intensity of each point divided by the corresponding C_2H_4 values as a function of time, since the equations predit essentially a first order dependence on C_2H_4. The slopes in the plots primarily describe the wall recombination rate constant and are weakly dependent on C_2H_4 and $\int Odt$ (see equation 11 of the previous section).

The time interpretation of the intercepts of Figures 10-11. has justified plotting equation (11a) in the described fashion.

$$I\big|_{t=0} = \frac{A\big|_{t=0}}{C_2H_4\big|_0}$$

Thus

$$I\big|_{t=0} = \frac{A\big|_{t=0}}{C_2H_4\big|_0} = \frac{A_n \cdot k_{18} \cdot k_1}{k_{10} \cdot k_9 \cdot O_2}$$

where

$I\big|_{t=0}$ is the ratio of intensity to concentration

-38-

$A|_{t=0}$ is defined in equation 12, and is not time dependent

$$\frac{k_{18}}{k_9} = \frac{I|_{t=0} \cdot k_{10} \cdot O_2}{O \cdot k_1 \cdot A_n}$$

where A_n is the Einstein coefficient associated with reaction 18. The obtained value for $\frac{k_{18}}{k_9} = 1.7$ supports the earlier postulate that $k_9 O_2 \gg k_{18} \cdot O$, or $O_2 \gg \frac{k_{18}}{k_9} \cdot O$ where the atomic oxygen concentration is 8μ in 80μ of O_2.

From the maximum CH_2O intensity observed k_3 was found to be 3×10^{-14}. The intensity at the 6th window was taken to be the highest that reaction (3) could produce,

$$k_3 = \frac{I_{ni} \cdot k'_1 \cdot k_{10}}{k_1 (e^{-\int k_{17} \cdot O \cdot dt} - e^{-\int k_1 O dt}) A_m}$$

where

$$I_{ni} = \frac{I_{limit}}{C_2H_4|_0}$$

and A_m is the associated Einstein coefficient with reaction 3.

The step calculations done for the above results are represented in Table IV.

The values for A_n and A_m used in this work were assumed to be 10 1/sec and 3.3 1/sec for reactions 18 and 3, respectively, guided by the exothermicity of the respective reactions. It is possible that the $OH^{\ddagger}$ emission is coming from a transition higher then the (1-0) transition, via reaction 18, while the smaller exothermicity of reaction 3 would justify using 3.3 1/sec (Potter, et al, 1970).
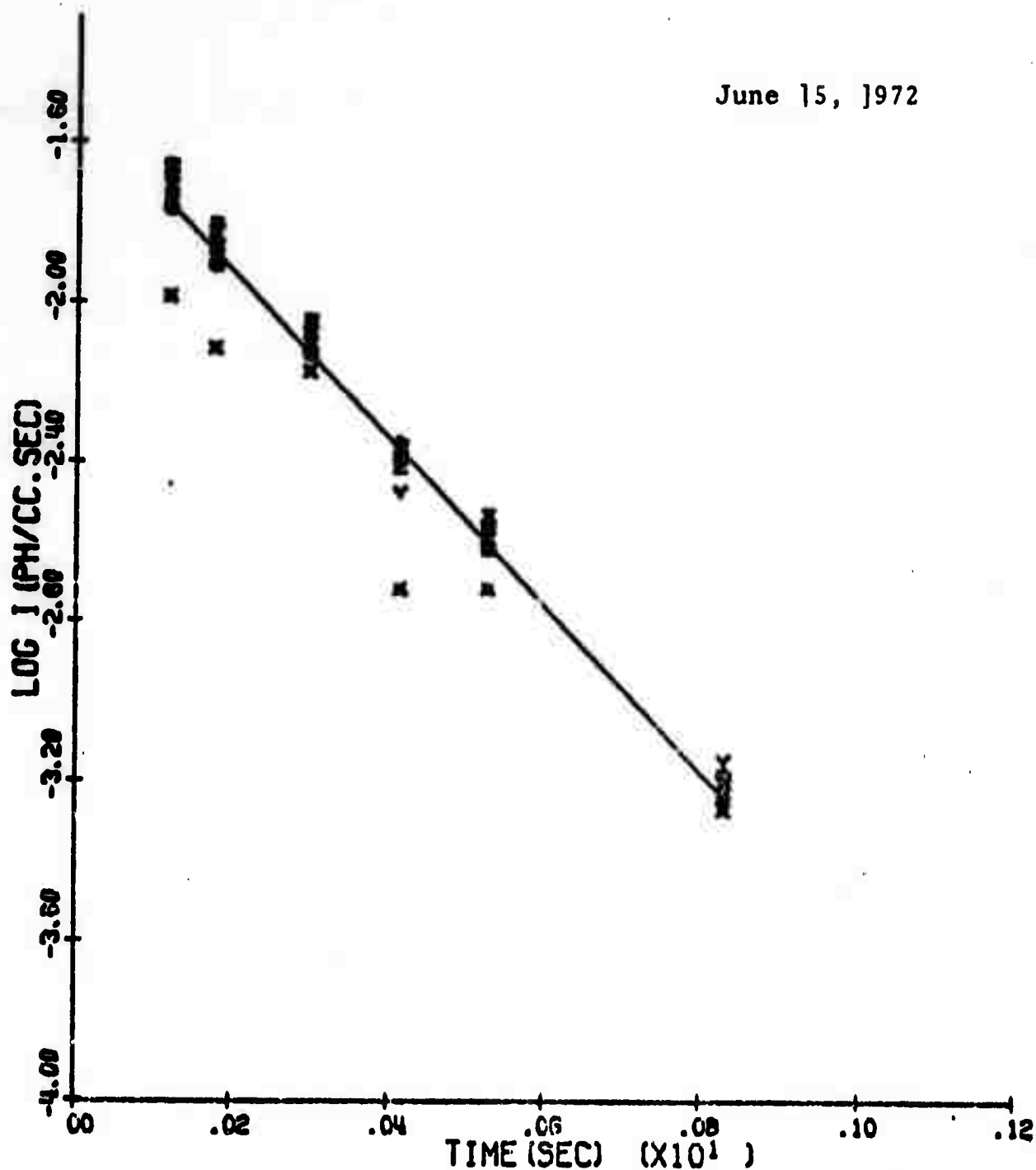
Figure 11. Log_{10} Intensity as a function of time. Each point was divided by its corresponding ethylene concentration, upon doing this almost all points corresponding to the same time overlapped. The slope of this curve mainly described the depletion of oxygen atoms.

-40-

Data Analysis

Date	$O_2(\mu)$	$O(\mu)$	$Log_{10} \frac{I}{C_2H_4}\big\|_0$ at t = 0	$\frac{k_{18}}{k_9}$	$Log_{10} \frac{I}{C_2H_4}$ at the last observation port	$k_3 A_m$	k_3 if $A_n = 3.3$
June 15, 1972	80	7.8	-1.5	1.90	-3.24	8.3×10^{-14}	2.5×10^{-14}
June 12, 1972	89	11.8	-1.36	1.90	-3.1	11.4×10^{-14}	3.42×10^{-14}
June 8, 1972	79	8	-1.59	1.50	-3.24	8.3×10^{-14}	2.5×10^{-14}
May 29, 1972	81	7.5	-1.62	1.54	-3.05	12.6×10^{-14}	3.78×10^{-14}

Thus, in summation, we have observed 2.7μ radiation emunating from the O + C_2H_4 reaction system which we attribute primarily to the reaction

$$CHO + O \rightarrow OH^{\ddagger} + CO \qquad (18)$$
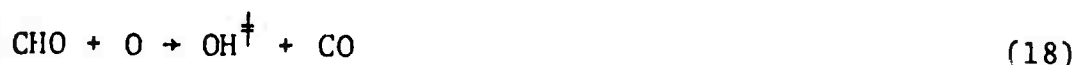
$OH^{\ddagger}$ is lost principally by reaction with oxygen atoms, through

$$OH^{\ddagger} + O \rightarrow O_2 + H; \qquad (10)$$

CHO must be lost principally via

$$CHO + O_2 \rightarrow products \qquad (9)$$

None of the rate constants needed here can be obtained uniquely from this study. However, the critical parameter in the study: $(\frac{k_{18}}{k_{10} \, k_9})$, can be determined by matching the experimental data extrapolated to zero contact time with the value $\frac{k_{18}}{k_{10} \, k_9}$.. Assuming that $OH^{\ddagger}$ reacts at the same rate as OH in the essentially gas kinetic reaction (10) producing O_2, we find that $k_{18}/k_9 = 1.7 \neq 0.2$. Using this ratio and the error limits, we can reproduce all the data theoretically to within the error limits.

REFERENCES

1. Aris, R., Elementary Chemical Reactor Analysis, Prentice Hall (1969).

2. Atkinson, R., and R. Cvetanovic, J. Chem. Phys. 56, 432 (1972).

3. Baulch, D., D. Drysdale, and A. Lloyd, Leeds Report Nos. 1-4, 1968.

4. Browne, W., R. Porter, J. Verlin, and A. Clark, Twelfth Symp. (Int.) on Combustion, the Combustion Institute, Pittsburgh, Pennsylvania, 1035 (1969).

5. Clyne, M., Ninth Symp. (Int.) on Combustion, The Combustion Inst., Pittsburgh, Pennsylvania, 211 (1963).

6. Davis, D., R. Huie, J. Herron, M. Kuryld, and W. Braun, J. Chem. Phys. 56, 4868 (1972).

7. Dixon-Lewis, G., Wilson, W.E., and Westenberg, J. Chem. Phys. 44, 2877 (1966).

8. Fontijn, A., C. Meyer, and H. Schiff, J. Chem. Phys. 40, 64 (1964).

9. Gutowski, R., Wayne State University Report, available from R. Kummler, (1971).

10. Herron, J., and R. Penzhorn, J. Phys. Chem. 73, 191 (1969).

11. Hershafar, F., J. Rogers, and A. T. Stair, Jr., Applied Optics 10, 1843 (1971).

12. Jonathan, N., C. Melliar-Smith, and D. Salter, Mol. Phys. 20, 93 (1971).

13. Kanofsky, J., D. Lucas, and D. Gutman, Fourteenth Symp. (Int.) on Combustion, preprint, 1972.

14. Kaufman, F., Ann. Geophys. $\underline{20}$, 106 (1964).

15. Keneshea, T., Air Force Cambridge Research Labs Report AFCRL-67-0221, April (1967).

16. Krieger, B., M. Malki, and R. Kummler, Environmental Science and Technology $\underline{6}$, to be published (1972).

17. Kummler, R. and M. Bortner, Proc. AMRAC Soc. $\underline{28}$ (1968).

18. Lloyd, A., NBS Report 10447 (1970).

19. McGrath, W., and R. Norrish, Proc. Roy. Soc. (London) $\underline{A242}$, 265 (1957).

20. Morris and Niki, private communication, 1971.

21. Niki, H., E. Daby, and B. Weinstock, Twelfth Symp. (Int.) on Combustion, The Combustion Institute, Pittsburgh, Pennsylvania, 277 (1969).

22. Pacey, P. and J. C. Polanyi, Appl. Opt. $\underline{10}$, 1725 (1971).

23. Parker, J., and G. Pimentel, J. Chem. Phys. $\underline{51}$, 91 (1969).

24. Potter, A., Jr., R. N. Coltharp, and S. Worley, J. Chem. Phys. $\underline{54}$, 992 (1970).

25. Renner, S., "Quantitative Molecular Spectroscopy and Gas Emissions" Addison Wesley, Reading Mass. (1959).

26. Roginski, G., Wayne State University Report, available from R. Kummler (1972).

27. Smith, I., to be published, 1972.

28. Stair, A. T., Jr., J. Kennealy, S. Stewart, Planet. Space Sci. $\underline{13}$, 1005 (1972).

29. Stair, A.T., Jr. and J. Kennealy, J. Chem. Phys. 124 (1967).

30. Stuhl, F., and H. Niki, J. Chem. Phys. $\underline{55}$, 3954 (1971).

31. Worley, S., R. Coltharp, and A. Potter, Jr., J. Phys. Chem. $\underline{76}$, 1511 (1972).

Part II: THEORETICAL DETERMINATION OF VIBRATIONAL EXCITATION
OF MOLECULES

R. Marriott

THEORETICAL DETERMINATION OF VIBRATIONAL EXCITATION OF MOLECULES

The theoretical program at RIES has been primarily concerned with the calculation of cross sections for the vibrational excitation of molecules by heavy body collisions. This is carried out using a numerical close coupling solution of the wave equation for the colliding system based on the breathing sphere model of Schwartz, Slawsky, and Herzfeld (1954) to represent the target molecular vibrator and an empirical spherically symmetric scattering potential, but neglecting any structure in the impacting particle.

For many gas mixtures of interest direct vibration - vibration (VV) energy transfer processes are also important. Nevertheless no calculations of such processes to the precision afforded by the close coupling approximation have been published up to the present time.

The RIES molecular collision code has now been extended to include vibrational states in the impacting particle. This in turn permits both the calculation of significant VV cross sections simultaneously with the VT cross sections within the same breathing sphere approximation, and the estimation of the effect produced on target particle VT cross sections by coupling in the impact particle states.

Calculations on the CO - CO system are currently underway to study the magnitude of VV cross sections for states in exact energy resonance and to determine the

effect of the impact particle states on the calculated VT cross section for the excitation of the first vibrational level of CO from the ground state. This cross section dominates the vibrational relaxation of CO, and since the previous VT results were in good agreement with experiment, the relevant cross section would not be expected to be particularly sensitive to the addition of impact particle states.

Preliminary results for collision systems in which coupling of both 2 and 3 states in the impacting and target particles has been retained are shown in Table I.

The cross section for the excitation of the first vibrational level is reduced by a factor of 2.5 from the corresponding 3 state calculation which ignores the structure in one particle. The VT cross section is reduced by a factor of 4 from the original 4 state results which give agreement with vibrational relaxation data. If a similar reduction occurs at all energies it would significantly affect the comparison of theory with experiment. However it can be seen that there are now additional competing process which must be taken into account. The energy exchange cross sections are very large. Clearly processes of the (V-V) type $CO(0) + CO(2) \rightarrow CO(1) + CO(1)$ will be orders of magnitude more effective in depopulating the higher vibrational states of CO than (V-T) processes such as

$$CO(0) + CO(2) \rightarrow CO(0) + CO(1) + .266eV.$$

The magnitude of the V-V cross sections in comparision

with V-T collisions is found to be caused by not only an increase in the individual partial cross sections, but also by the fact that of the order of twice as many (300:150) partial waves contribute significantly to the (V-V) total. This re-emphasizes the long range nature of the V-V interaction in a very concrete way.

While the results obtained so far seem reasonable, they must be regarded as tentative since it is evident that a sufficient number of molecular states to ensure convergence of the cross sections have not yet been coupled together.

It was shown in the original CO-CO (V-T) calculation that 4 or 5 states had to be included for convergence. Unfortunately, as presently constructed, the molecular code will not handle the case of virtual states; all coupled states must be energetically accessible.

This means that for any specific selection of excited states there is a certain collision energy threshold below which the code cannot be run. This was not an important restriction for the V-T calculation where only one excited particle was considered. For the new V-V code with both particles excited however it is more serious. Indeed including 5 states in each CO molecule would prevent the code being run at a collision energy less than 2.7 eV, outside the region of interest for many purposes.

It is necessary therefore to further extend the code

Table I. Inelastic cross sections (in units of πa_0^2) for CO-CO collisions at a total system energy of 1.5 eV.

Collision process		Zero order partial cross section			
$A(i)+B(n)$ $\rightarrow$	$A(j)+B(m)$	Number coupled states $\begin{cases} A(0) \\ B(0,1,2) \end{cases}$	(0) $(0,1,2,4)$	$(0,1)$ $(0,1)$	$(0,1,2)$ $(0,1,2)$
† CO(0)+CO(0)+1.5eV $\rightarrow$	CO(0)+CO(0)+1.234eV	$.8\times10^{-2}$	$.12\times10^{-1}$	$.21\times10^{-2}$	$.32\times10^{-2}$
$\rightarrow$	CO(1)+CO(0)+1.234eV				
CO(0)+CO(0)+1.5eV $\rightarrow$	CO(1)+CO(0)+.968eV	-----	-----	$.16\times10^{-6}$	$.2\times10^{-5}$
$\rightarrow$	CO(2)+CO(0)+.968eV	-----	$.17\times10^{-5}$	-----	$.4\times10^{-6}$
* $\begin{cases}$ CO(0)+CO(2)+.968eV $\rightarrow$	CO(1)+CO(1)+.968eV	-----	-----	-----	.9
CO(0)+CO(1)+1.234eV$\rightarrow$	CO(1)+CO(0)+1.234eV	-----	-----	.54	.7
CO(0)+CO(2)+.968eV $\rightarrow$	CO(0)+CO(1)+1.234eV	-----	$.44\times10^{-2}$	-----	$.22\times10^{-2}$

* Exact resonance energy exchange processes.

† Process dominating vibrational relaxation of CO.

-49-

to accept the case of virtual states. Although this poses no analytic problem, indeed close coupling electron scattering codes are so constructed, it will require a fairly extensive re-ordering of the program subroutines and particularly the treatment of the asymptotic solutions. This program extension is now underway and when operational the CO-CO test calculation will be completed.

Part III: DETERMINATION OF THE INTERMOLECULAR POTENTIAL
BY MOLECULAR BEAM METHODS

P. Foreman and P. Rol

A molecular beam apparatus donated by NASA is being used to measure the intermolecular potentials required as input for close coupled calculations of excitation cross sections. A number of improvements to the apparatus have been necessary; these include the substitution of a low energy electron bombardment ion source and improved lens system which provides a stable beam with very low energy spread. In addition the scattering gas handling system has been reconstructed to eliminate the effects of surface outgassing and pressures are measured with a capacitance manometer calibrated against a McLeod gauge.

Preliminary experiments with the Ar-Ar system yielded potentials which were not fully in agreement either with theory or with previous experimental determinations. Thus, in order to check that the apparatus and the analysis programs are functioning correctly, we have measured the potential for the He-He interaction, for which highly reliable calculations have been made {1,2}. For this system, incomplete total cross sections were measured as a function of relative energy with various scattering geometrics.

We have restricted our attention to the case where the diameter of the detector p is larger than that of the beam d since this provides more signal and also simplifies the analysis. Jordan and Amdur have shown {3} that the measured cross section is a maximum when d=p and decreases

asymptotically as d/p tends to zero or infinity; a comparison
of curves I and III in Figure 1 confirms their finding.
These were measured with a thermopile, the closed symbols
denoting its conventional application in which the beam transfers
its kinetic energy to the detector and produces a potential
difference across the junction due to the Peltier effect.
Such measurements require proper matching of the low source
impedance with the input of the amplifier; if the signal is
placed across a high impedance input then the secondary electron
emission is measured (open symbols in Fig. 1) with a gain
increased by a factor of 3000. To further entend the range of
measurement at low energies, a channeltron electron multiplier
has been used and the results are shown as curve II, Figure 1
for an intermediate value of d/p. Inversion of these curves
produces potentials which are virtually indistinguishable
from the best theoretical result of Yilbert and Wahl {1}, and
to avoid confusion only one is plotted in Figure 2. An
earlier theoretical result of Phillipson {2} is similarly close
whereas the best previous experimental results of Jordan and
Andrew {3}, and Kammer and Leonas {4} also shown in Figure
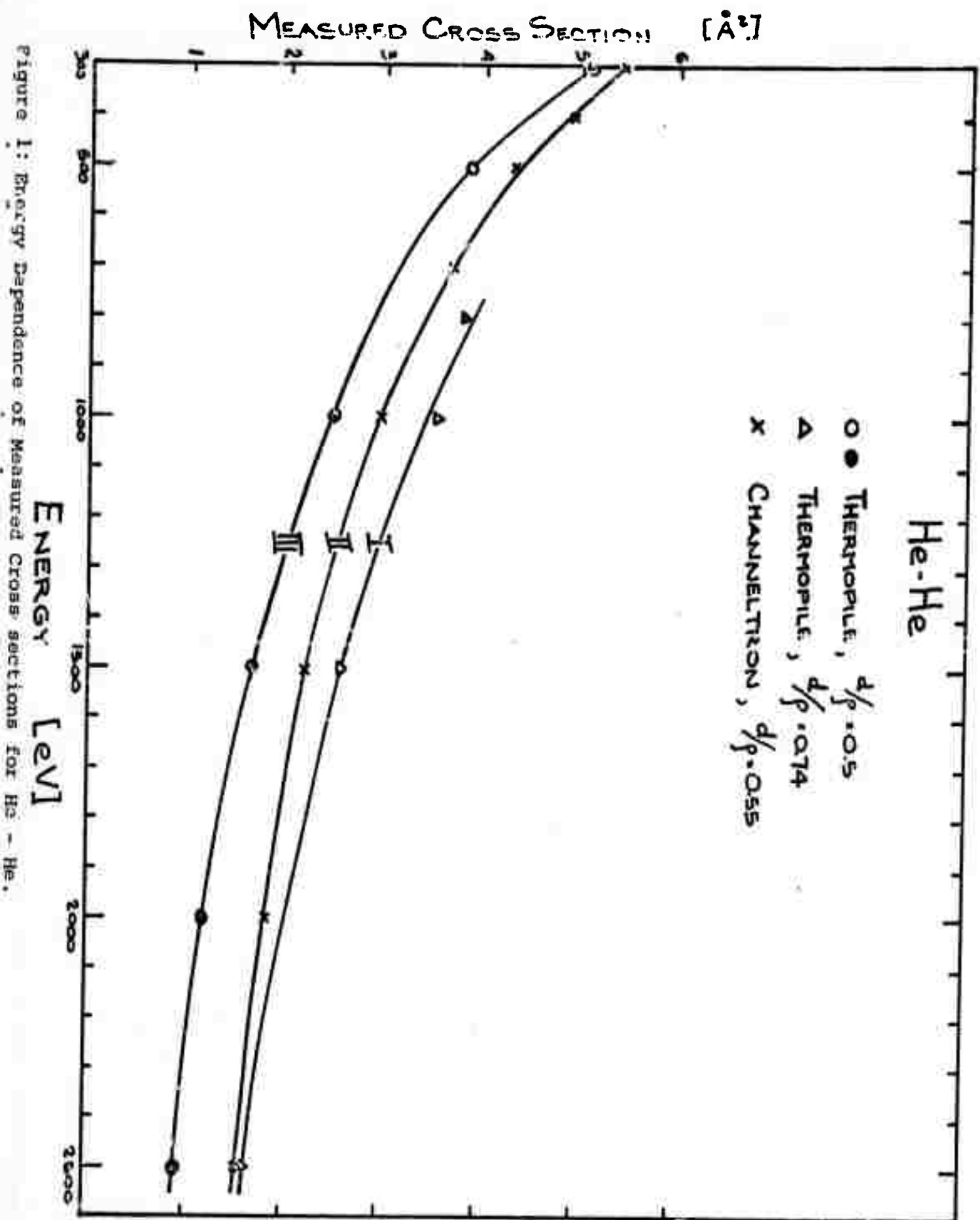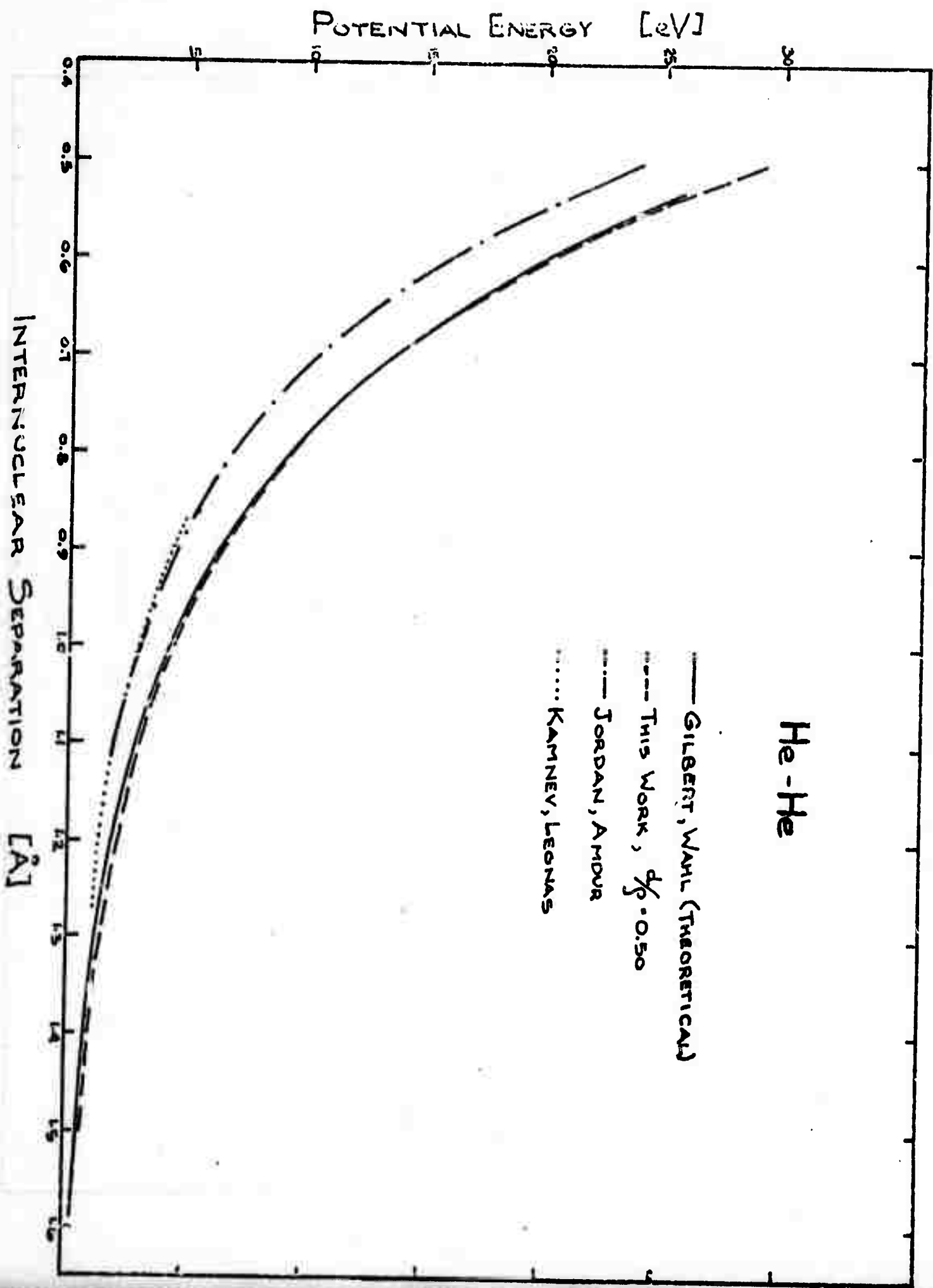2 are distinctly lower.

Figure 1: Energy Dependence of Measured Cross sections for He — He.

POTENTIAL ENERGY [eV]

INTERNUCLEAR SEPARATION [Å]

He-He

—— GILBERT, WAHL (THEORETICAL)

—·— THIS WORK, $\frac{d}{p} = 0.50$

— — JORDAN, AMDUR

······ KAMNEV, LEONAS

We therefore feel confident to proceed with systems for which there is a theoretical check and are currently investigating the potential for the Ar-Co interaction. It is hoped that this, **together with the** potential for O atoms with exhaust plume species will soon be available.

References

(1) Yilbert, T.L., Wahl, A.C.; J. Chem. Phys. <u>47</u>, 3425, (1967)

(2) Phillipson, P.E.; Phys. Rev. <u>125</u>, 1981, (1962)

(3) Jordan, J.E., Amdur, 1.; J. Chem. Phys. <u>46</u>, 165, (1967)

(4) Kamner, A.B., Leonas, V.B.; Sov. Phys. Doklady <u>10</u>, 529, (1965)